

Femtosecond valley polarization and topological resonances in transition metal dichalcogenides

S. Azar Oliaei Motlagh, Jhih-Sheng Wu, Vadym Apalkov, and Mark I. Stockman

Center for Nano-Optics (CeNO) and Department of Physics and Astronomy, Georgia State University, Atlanta, Georgia 30303, USA

(Received 27 November 2017; revised manuscript received 5 August 2018; published 15 August 2018)

We theoretically introduce the fundamentally fastest induction of a significant population and valley polarization in a monolayer of a transition metal dichalcogenide (i.e., MoS₂ and WS₂). This may be extended to other two-dimensional materials with the same symmetry. This valley polarization can be written and read out by a pulse consisting of just a single optical oscillation with a duration of a few femtoseconds and an amplitude of ~ 0.25 V/Å. Under these conditions, we predict an effect of *topological resonance*, which is due to the Bloch motion of electrons in the reciprocal space where electron population textures are formed due to non-Abelian Berry curvature. The predicted phenomena can be applied for information storage and processing in PHz-band optoelectronics.

DOI: [10.1103/PhysRevB.98.081406](https://doi.org/10.1103/PhysRevB.98.081406)

Femtosecond and attosecond technology has made it possible to control and study ultrafast electron dynamics in three-dimensional solids [1–6]. There is a wide class of two-dimensional (2D) crystals, which have unique and useful properties [7–14] that bear a promise for applications in ultrafast optoelectronics [15]. However, not all 2D materials are suitable for any given application. For example, graphene is a well-studied 2D material, which is semimetallic with no band gap between the valence band (VB) and the conduction band (CB). This causes a relatively high off-current in graphene transistors, drastically limiting their usefulness [16–19]. In contrast, there is a broad class of 2D semiconductors possessing finite direct band gaps. Among them, transition metal dichalcogenides (TMDCs) possess direct band gaps of 1.1–2.1 eV [7,10,11,20–22].

Similar to graphene, TMDC monolayers have hexagonal lattices formed by two triangular sublattices [10,18,20]. Unlike graphene, these sublattices consist of different atoms (metal and chalcogen), which break the inversion (\mathcal{P}) symmetry and open up band gaps at the K , K' points whose degeneracy is protected by time-reversal (\mathcal{T}) symmetry [18,23].

The \mathcal{T} symmetry and K , K' -valley degeneracy can be relaxed by circularly polarized optical pumping, which allows for a highly valley-specific electron population, depending on the helicity of the excitation pulse [21,23–27]. This selective valley population, known as valley polarization, introduces a new area referred to as valleytronics [12,28]. A significant spin-orbit coupling (SOC) makes these materials promising also for spintronics [21,25].

In this Rapid Communication, we theoretically introduce the fundamentally fastest induction of significant population and valley polarization in MoS₂ and WS₂ monolayers by a *single* cycle of a strong circularly polarized optical field with a duration of a few femtoseconds and an amplitude of $0.2\text{--}0.5$ V Å⁻¹. This process is determined by electron motion in the reciprocal space, spanning a significant part of the Brillouin zone. This motion also causes an effect, called *topological resonance*, which we introduce below in the discussion of Fig. 1.

For a single-oscillation pulse, the optical electric field $\mathbf{F}(t)$ as a function of time t is parametrized as

$$F_x(t) = F_0(1 - 2u^2)e^{-u^2}, \quad F_y(t) = \pm 2uF_0e^{-u^2}, \quad (1)$$

where $u = t/\tau$, and $\tau = 1$ fs determines the pulse duration and its mean frequency [see Supplemental Material (SM) [29] for the definition] $\hbar\bar{\omega} \approx 1.2$ eV. The \pm sign defines helicity of the applied pulse: + for right-handed and – for left-handed circular polarization. These left- and right-handed pulses are mutually \mathcal{T} reversed. A few- or single-oscillation pulses are presently experimentally available from the near-ultraviolet through the terahertz range in linear [30–36] or circular polarization [35,37].

We set the TMDC monolayer in the xy plane with the pulse incident in the z direction. We use a three-band tight-binding (TB) (third-nearest-neighbor) model Hamiltonian [20] H^{TNN} [see Eq. (1) of SM].

The TB Hamiltonian of a TMDC monolayer is composed by three orbitals, d_{z^2} , d_{xy} , and $d_{x^2-y^2}$, of the metal atom. The full Hamiltonian is $H(t) = H^{\text{TNN}} + H^{\text{SOC}} + H^{\text{int}}(t)$, where H^{SOC} is the SOC term [Eq. (3) of SM], and $H^{\text{int}}(t)$ is the light-TMDC interaction term. In the length gauge, $H^{\text{int}} = -e\mathbf{F}(t)\mathbf{r}$, where e is the electron charge. This model includes three bands, valence band (VB) and two conduction bands (CBs), each band spin split into two bands.

We assume that electron collisions can be neglected because the applied pulse (a few femtoseconds) is much shorter than the electron scattering (dephasing) time in TMDCs. In fact, this dephasing time was 500 fs for an atomically thin MoS₂ [38]. Also, Ref. [39] reported electron coherence times for WSe₂ to be 150–410 fs. In Ref. [40], the dephasing time was calculated to be ≈ 37 fs for a few layers of MoS₂. The carrier relaxation time in MoS₂ was found to be 25 ps, and the electron-hole recombination time to be 300 ps [41]. Based on this, we describe the electron dynamics as coherent by the time-dependent Schrödinger equation (TDSE). Previously, such a TDSE theory [42–50] was successful in predicting new effects and describing experimental results in both three-dimensional solids [2,3,51] and graphene [52]. For noninteracting particles,

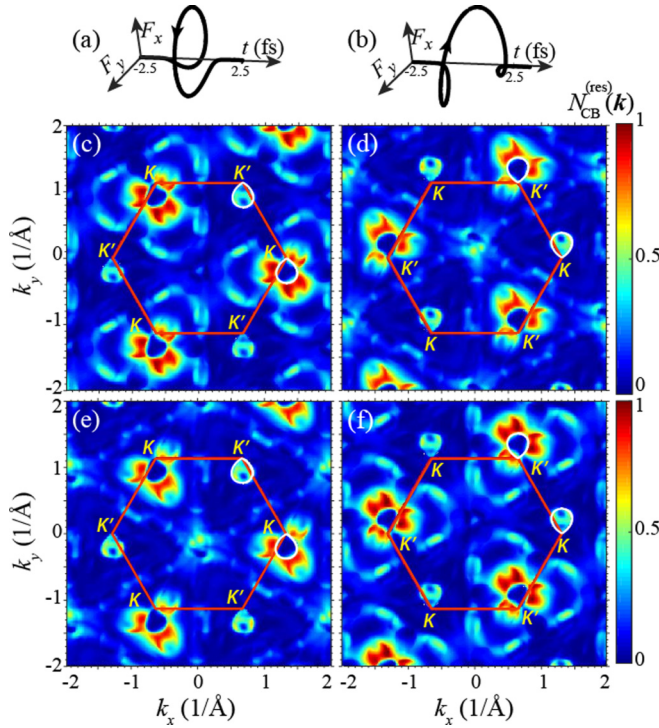


FIG. 1. Residual CB population $N_{\text{CB}}^{(\text{res})}(\mathbf{k})$ for monolayer MoS₂ in the extended zone picture. The red solid line shows the first Brillouin zone boundary with K, K' points indicated. The amplitude of the optical field is $F_0 = 0.25 \text{ V \AA}^{-1}$. (a) Wave form $\mathbf{F}(t)$ for a right-handed circularly polarized pulse. (b) The same as (a) but for a left-handed circularly polarized pulse [\mathcal{T} reversed to that in (a)]. (c) Residual population of spin-up electrons $N_{\text{CB}_1}^{(\text{res})}(\mathbf{k})$ for a right-handed pulse. (d) The same as (c) $N_{\text{CB}_1}^{(\text{res})}(\mathbf{k})$ but for a left-handed pulse. (e) Residual population of spin-down electrons $N_{\text{CB}_2}^{(\text{res})}(\mathbf{k})$ for a right-handed pulse. (f) The same as (e) $N_{\text{CB}_2}^{(\text{res})}(\mathbf{k})$ but for a left-handed pulse.

the TDSE theory is fundamentally equivalent to the density matrix equations but is computationally much more efficient.

In solids, an applied electric field generates both intraband and interband electron dynamics. The intraband dynamics is determined by the Bloch acceleration theorem [53]: For an electron with an initial crystal momentum \mathbf{q} , the time-dependent crystal momentum $\mathbf{k}(\mathbf{q}, t)$ is

$$\mathbf{k}(\mathbf{q}, t) = \mathbf{q} + \frac{e}{\hbar} \int_{-\infty}^t \mathbf{F}(t') dt'. \quad (2)$$

The corresponding wave functions, which are solutions of the TDSE,

$$i\hbar \frac{d\Psi}{dt} = H(t)\Psi, \quad (3)$$

within a single band α , are the well-known Houston functions [54],

$$\Phi_{\alpha\mathbf{q}}^{(H)}(\mathbf{r}, t) = \Psi_{\mathbf{k}(\mathbf{q}, t)}^{(\alpha)}(\mathbf{r}) e^{-\frac{i}{\hbar} \int_{-\infty}^t dt_1 E_{\alpha}[\mathbf{k}(\mathbf{q}, t_1)]}, \quad (4)$$

where $\alpha = v, c_1, c_2$ for the VB and CBs, correspondingly, $\Psi_{\mathbf{k}}^{(\alpha)}$ are Bloch-band eigenfunctions in the absence of the pulse field, and $E_{\alpha}(\mathbf{k})$ is the band energy.

The interband electron dynamics is determined by the solution $\Psi_{\mathbf{q}}(\mathbf{r}, t)$ of TDSE (3), which can be expressed in the basis of the Houston functions $\Phi_{\alpha\mathbf{q}}^{(H)}(\mathbf{r}, t)$,

$$\Psi_{\mathbf{q}}(\mathbf{r}, t) = \sum_{\alpha=c,v} \beta_{\alpha\mathbf{q}}(t) \Phi_{\alpha\mathbf{q}}^{(H)}(\mathbf{r}, t), \quad (5)$$

where $\beta_{\alpha\mathbf{q}}(t)$ are expansion coefficients.

Let us introduce the following quantities,

$$\mathcal{A}'_{\alpha'\alpha}(\mathbf{q}, t) = \mathcal{A}_{\alpha'\alpha}[\mathbf{k}(\mathbf{q}, t)] \exp[i\phi'_{\alpha'\alpha}(\mathbf{q}, t)], \quad (6)$$

$$\phi'_{\alpha'\alpha}(\mathbf{q}, t) = \frac{1}{\hbar} \int_{-\infty}^t dt' (E_{\alpha'}[\mathbf{k}(\mathbf{q}, t')] - E_{\alpha}[\mathbf{k}(\mathbf{q}, t')]), \quad (7)$$

$$\mathcal{A}_{\alpha'\alpha}(\mathbf{q}) = \left\langle \Psi_{\mathbf{q}}^{(\alpha')} \left| i \frac{\partial \Psi_{\mathbf{q}}^{(\alpha)}}{\partial \mathbf{q}} \right. \right\rangle, \quad \mathbf{D}_{\alpha'\alpha}(\mathbf{q}) = e \mathcal{A}_{\alpha'\alpha}(\mathbf{q}). \quad (8)$$

Here, $\alpha, \alpha' = v, c_1, c_2$ are band indices, $\alpha \neq \alpha'$; $\mathcal{A}_{\alpha'\alpha}(\mathbf{q})$ is a matrix element of the non-Abelian Berry connection [55–57], $\mathbf{D}_{\alpha'\alpha}(\mathbf{q})$ is the interband dipole matrix element, and $\phi'_{\alpha'\alpha}(\mathbf{q}, t)$ is the dynamic phase.

We introduce TDSE in the interaction representation in the adiabatic basis of the Houston functions as

$$i\hbar \frac{\partial B_{\mathbf{q}}(t)}{\partial t} = H'(\mathbf{q}, t) B_{\mathbf{q}}(t), \quad (9)$$

where the wave function (vector of state) $B_{\mathbf{q}}(t)$ and Hamiltonian $H'(\mathbf{q}, t)$ are defined as

$$B_{\mathbf{q}}(t) = \begin{bmatrix} \beta_{c_2\mathbf{q}}(t) \\ \beta_{c_1\mathbf{q}}(t) \\ \beta_{v\mathbf{q}}(t) \end{bmatrix}, \quad (10)$$

$$H'(\mathbf{q}, t) = -e\mathbf{F}(t) \hat{\mathcal{A}}(\mathbf{q}, t), \quad (11)$$

$$\hat{\mathcal{A}}(\mathbf{q}, t) = \begin{bmatrix} 0 & \mathcal{A}'_{c_2c_1}(\mathbf{q}, t) & \mathcal{A}'_{c_2v}(\mathbf{q}, t) \\ \mathcal{A}'_{c_2c_1}^*(\mathbf{q}, t) & 0 & \mathcal{A}'_{c_1v}(\mathbf{q}, t) \\ \mathcal{A}'_{c_2v}^*(\mathbf{q}, t) & \mathcal{A}'_{c_1v}^*(\mathbf{q}, t) & 0 \end{bmatrix}. \quad (12)$$

Matrix $\hat{\mathcal{A}}(\mathbf{q}, t)$ is the non-Abelian Berry connection in the interaction representation. The Schrödinger equation (9) defines the dynamics of the system with accuracy limited by the truncation of the Hilbert space.

Using Eq. (2), a general solution of Eq. (9) can be presented in terms of the evolution operator $\hat{S}(\mathbf{q}, t)$ as

$$B_{\mathbf{q}}(t) = \hat{S}(\mathbf{q}, t) B_{\mathbf{q}}(-\infty), \quad (13)$$

$$\hat{S}(\mathbf{q}, t) = \hat{T} \exp \left[i \int_{t'=-\infty}^t \hat{\mathcal{A}}(\mathbf{q}, t') d\mathbf{k}(\mathbf{q}, t') \right], \quad (14)$$

where \hat{T} is the time-ordering operator [58], and the integral is affected along the Bloch trajectory $\mathbf{k}(\mathbf{q}, t)$ [Eq. (2)].

We numerically solve TDSE (9) with initial conditions $\beta_{v\mathbf{q}}(-\infty) = 1, \beta_{c_1\mathbf{q}}(-\infty) = 0, \beta_{c_2\mathbf{q}}(-\infty) = 0$. The total population of the CBs is $N_{\text{CB}}(\mathbf{q}, t) = |\beta_{c_1\mathbf{q}}(t)|^2 + |\beta_{c_2\mathbf{q}}(t)|^2$. After the pulse ends, there remains a residual CB population $N_{\text{CB}}^{(\text{res})}(\mathbf{q}) = N_{\text{CB}}(\mathbf{q}, \infty)$.

The field of a single-oscillation right-handed circularly polarized pulse [see Eq. (1)] is displayed in Fig. 1(a) and the \mathcal{T} -reversed, left-handed pulse in Fig. 1(b). The residual

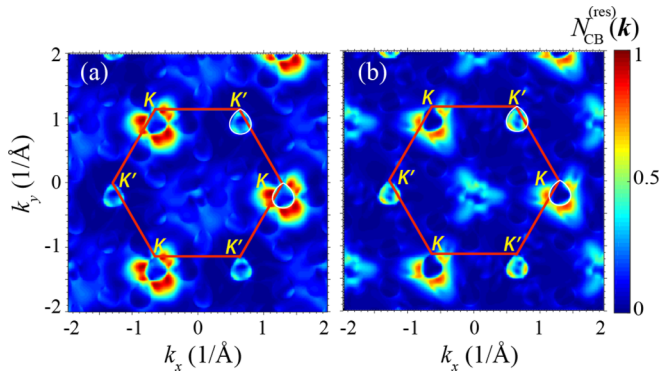


FIG. 2. Residual CB populations $N_{\text{CB}}^{(\text{res})}(\mathbf{k})$ for monolayer WS_2 after a right-handed circularly polarized pulse. Note that the corresponding distributions for a left-handed pulses are related to these by the \mathcal{T} symmetry similar to Fig. 1. The red solid line shows the Brillouin zone boundary. Amplitude of the applied field is $F_0 = 0.25 \text{ V \AA}^{-1}$. (a) Population $N_{\text{CB}\downarrow}^{(\text{res})}(\mathbf{k})$ for spin-up electrons. (b) The same as (a) but for spin-down electrons $N_{\text{CB}\uparrow}^{(\text{res})}(\mathbf{k})$.

CB population for MoS_2 induced by such a pulse with an amplitude of $F_0 = 0.25 \text{ V \AA}^{-1}$ is displayed in Figs. 1(c) and 1(d) for spin up ($s_z = 1/2$ or \uparrow) and Figs. 1(e) and 1(f) for spin down ($s_z = -1/2$ or \downarrow). Valley polarization is high: The right-handed pulse populates predominantly the K valleys, while the left-handed pulse excites mostly the K' valleys. Protected by the \mathcal{T} symmetry, the K_{\uparrow} -valley population for a given handedness pulse is inverted ($\mathbf{k} \leftrightarrow -\mathbf{k}$) to the K'_{\downarrow} -valley population for the opposite handedness; the same is true for K_{\downarrow} and K'_{\uparrow} . Correspondingly, Fig. 1(c) is center reflected to Fig. 1(f), and Figs. 1(d) to 1(e). The valley polarization is large, $\eta_V \gtrsim 40\%–60\%$ for at $F_0 = 0.1–0.25 \text{ V \AA}^{-1}$ —see Sec. VI of SM. There is also an appreciable, though smaller, spin polarization due to SOC.

We also performed computations for a two-oscillation pulse (see SM Fig. 3) and found no fundamental difference from the single-oscillation pulses. In fact, both the valley polarization and CB population become higher.

The valley and spin polarization in TMDCs caused by relatively weak (perturbative) circularly polarized continuous-wave (cw) radiation [21,24,25] or relatively long 30-fs pulses [41] were previously known and attributed to angular momentum conservation at the K, K' points [21,26]. The spin polarization is related to the intrinsic SOC in the transition metals [20,21,26].

A distinction of this Rapid Communication is that the significant CB population and valley polarization (along with a smaller spin polarization) can be written by a *single-oscillation* strong chiral pulse. The readout can also be done by a single-oscillation chiral pulse: Optical absorption of the readout pulse of the same chirality will be reduced due to the Pauli blocking, while the opposite-chirality pulse absorption will not be attenuated because it interacts with the other, unpopulated valley. This one-optical-cycle recording and readout make a basis of a fundamentally fastest optical memory.

Figures 2(a) and 2(b) illustrate the residual CB population for another TMDC, WS_2 , after a right-handed circularly

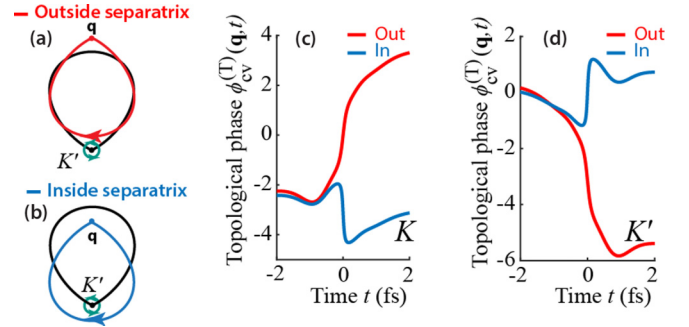


FIG. 3. For a chiral left-handed pulse, Bloch trajectories $\mathbf{k}(\mathbf{q}, t)$ in the K' valley and topological phase $\phi_{cv}^{(T)}(\mathbf{q}, t)$ for transitions $v \rightarrow c$ between bands forming the band gaps at the K and K' points. (a) Separatrix for the pulse used is shown by the black line. Electron Bloch trajectory $\mathbf{k}(\mathbf{q}, t)$ is shown for an initial point \mathbf{q} outside the separatrix. The K' point is denoted by a solid dot and the Berry connection is denoted by a green “whirl” where the chirality is indicated by arrows. (b) The same as (a) but for \mathbf{q} inside the separatrix. (c) Topological phase $\phi_{cv}^{(T)}(\mathbf{q}, t)$ on the Bloch trajectory for the K point and \mathbf{q} outside of the separatrix (red line) and inside the separatrix (blue line). (d) The same as (c) but for the K' point.

polarized pulse with an amplitude of $F_0 = 0.25 \text{ V \AA}^{-1}$ for spin-up and spin-down electrons, respectively. Similar to Fig. 1, the right-handed single-oscillation pulse populates predominantly the K valleys. Due to stronger SOC in W in comparison to Mo, the spin dependence is more pronounced.

The known valley selection rules for chiral pulses [21,23–27,59] are angular momentum perturbative selection rules, which are local in \mathbf{k} . In contrast, there is also a fundamentally different, nonlinear-optical selection rule characteristic of strong-field excitation, which is evident from Figs. 1 and 2: In all cases when a given valley is favored by the angular momentum selection rule, its population predominantly occurs *outside* of a closed curve (called the separatrix [48]). This is the case for K valleys in Figs. 1(c), 1(e) and 2 and for the K' valleys in Figs. 1(d) and 1(f). In the opposite case, when the angular momentum selection rule suppresses a valley’s population, then the momentum states *inside* the separatrix are predominantly but weakly populated as is the case for the K' valleys in Figs. 1(c), 1(e), and 2 and the K valleys in Figs. 1(d) and 1(f).

The formation of such textures is a fundamental effect, which is nonlocal in \mathbf{k} and directly related to the global topology of the Bloch bands. It is inherent in the strong-field excitation where an electron moves in the reciprocal space exploring the non-Abelian Berry connection $\hat{\mathbf{A}}(\mathbf{k})$ along its Bloch trajectory—cf. Eq. (14). We call it *topological resonance*.

To understand the topological resonance, we turn to Figs. 3(a) and 3(b). The separatrix, which is shown by a solid black line, is defined as a set of initial points \mathbf{q} for which electron trajectories pass precisely through the corresponding K or K' points [48]. Its parametric equation is $\mathbf{q}(t) = \mathbf{K} - \mathbf{k}(0, t)$, or $\mathbf{q}(t) = \mathbf{K}' - \mathbf{k}(0, t)$ where $t \in (-\infty, \infty)$ is a parameter. For an initial crystal momentum \mathbf{q} outside of the separatrix, the electron trajectory $\mathbf{k}(\mathbf{q}, t)$ does not encircle the K point as in Fig. 3(a), otherwise it does as in Fig. 3(b).

The evolution operator of Eq. (14) describes a deeply nonlinear, complex quantum dynamics of the photoexcitation whose exact evaluation can only be done numerically (cf. Figs. 1 and 2 above). To get a qualitative insight, consider Eq. (14) in the first order of perturbation theory, where it becomes

$$\hat{S}(\mathbf{q}, t) = 1 + i \int_{t'=-\infty}^t \hat{\mathcal{A}}(\mathbf{q}, t') d\mathbf{k}(\mathbf{q}, t'). \quad (15)$$

Correspondingly, the residual (after the pulse ends) CB population n_α is

$$n_\alpha = \left| \oint |\mathcal{A}_{\alpha v}[\mathbf{k}(\mathbf{q}, t)]\mathbf{n}(t)| \exp[i\phi_{\alpha v}^{(\text{tot})}(\mathbf{q}, t)] d\mathbf{k}(\mathbf{q}, t) \right|^2, \quad (16)$$

where $\alpha = c_1, c_2$, and the integral is affected along a closed-loop Bloch trajectory (2) whose parametric form is $\mathbf{k}(\mathbf{q}, t)$ with parameter $t \in \{-\infty, \infty\}$, $\mathbf{n}(t) = \mathbf{F}(t)/F(t)$ is the unit vector tangential to the Bloch trajectory, the total phase $\phi^{(\text{tot})}$ is expressed as

$$\phi_{\alpha v}^{(\text{tot})} = \phi_{\alpha v}^{(\text{T})}(\mathbf{q}, t) + \phi_{\alpha v}^{(\text{d})}(\mathbf{q}, t), \quad (17)$$

and topological phase is defined as

$$\phi_{\alpha v}^{(\text{T})}(\mathbf{q}, t) = \arg \{ \mathcal{A}_{\alpha v}[\mathbf{k}(\mathbf{q}, t)]\mathbf{n}(t) \}. \quad (18)$$

Note that the non-Abelian Berry connection element $\mathcal{A}_{\alpha v}[\mathbf{k}(\mathbf{q}, t)]$ and the topological phase $\phi_{\alpha v}^{(\text{T})}(\mathbf{q}, t)$ are not gauge invariant, and, correspondingly, are not observable. However, the CB population n_α , as given by a closed-loop integral of Eq. (16), is observable. Also, the total change of the topological phase during the pulse $\Delta\phi_{\alpha v}^{(\text{T})}(\mathbf{q}) = \phi_{\alpha v}^{(\text{T})}(\mathbf{q}, \infty) - \phi_{\alpha v}^{(\text{T})}(\mathbf{q}, -\infty)$ can be observed interferometrically in a two-cycle experiment as proposed earlier [48]. It is, therefore, also gauge invariant.

The topological phase $\phi_{\alpha v}^{(\text{T})}(\mathbf{q}, t)$ (18) is displayed in Fig. 3(c) for the K valley and in Fig. 3(d) for the K' valley. The total changes of this phase for the valleys with opposite chiralities are opposite, as protected by the \mathcal{T} symmetry. For the initial crystal momentum \mathbf{q} outside of the separatrix, this change is significantly larger in magnitude than when it is inside the separatrix (cf. the red versus blue lines) and is close to $\pm 2\pi$.

In Eq. (16), modulus $|\mathcal{A}_{\alpha v}[\mathbf{k}(\mathbf{q}, t)]\mathbf{n}(t)|$ is a smooth function of time; it is the oscillating phase factor $\exp[i\phi_{\alpha v}^{(\text{tot})}(\mathbf{q}, t)]$ that determines whether the integral is large or small. If the topological phase $\phi_{\alpha v}^{(\text{T})}(\mathbf{q}, t)$ and the dynamic phase $\phi_{\alpha v}^{(\text{d})}(\mathbf{q}, t)$ mutually cancel each other in Eq. (17), then the accumulation along the Bloch trajectory in the integral of Eq. (16) is coherent, and n_α is large. If to the opposite, the dynamic phase and topological phase add to each other, then the phase exponential in Eq. (16) oscillates more rapidly, and the contributions along the Bloch trajectory tend to mutually cancel each other, leading to a small value of n_α .

Under resonant conditions, the dynamic phase $\phi_{\alpha v}^{(\text{d})}(\mathbf{q}, t)$ [Eq. (7)] during the pulse monotonically increases with time t by $\approx 2\pi$. Hence, the topological resonance takes place for the topological phase $\phi_{\alpha v}^{(\text{T})}(\mathbf{q}, t)$, decreasing by the same amount, $\Delta\phi_{\alpha v}^{(\text{T})} \approx -2\pi$. For the case of a left-handed pulse illustrated in Fig. 3, this topological resonance occurs for the crystal momentum \mathbf{q} outside of the separatrix for the K' point [see the red curve in Fig. 3(d)].

For the same example of a left-handed pulse illustrated in Fig. 3, if \mathbf{q} is inside the separatrix, then the change of the topological phase during the pulse for the K point is $\Delta\phi_{\alpha v}^{(\text{T})} \approx -\pi$. In such a case, there is only a partial phase compensation. This leads to a weak population of the K valley inside the separatrix. This qualitative picture is precisely what one can see in Figs. 1(d) and 1(f): a strong population of the K' valley outside of the separatrix and a weak population of the K valley inside the separatrix. Note that the topological resonance only weakly depends on spin [Figs. 1(d) and 1(f) are very similar], because the SOC is still relatively weak. Protected by the \mathcal{T} -reversal symmetry, for the opposite chirality of the pulse, the K and K' valleys are exchanged, and the spin is changed to the opposite—cf. Figs. 1(d) and 1(f) with Figs. 1(c) and 1(e). These properties of the topological resonance are general for all TMDCs—cf. Figs. 1(c) and 1(e) with Figs. 2(a) and 2(b).

To conclude, we have demonstrated a fundamental possibility to induce a significant CB population and valley polarization in TMDCs during just one optical period of a chiral, moderately-high-field ($F_0 \sim 0.25$ V/Å) laser pulse. This is a wideband ultrafast process which is defined by the topological resonance that we have introduced above. This resonance is due to a mutual compensation of the dynamic phase and the non-Abelian Berry phase, which brings about the formation of textures in the \mathbf{k} space with discontinuities at the separatrices. These textures can be directly observed using time-resolved angle-resolved photoelectron spectroscopy [60].

The topological resonances can be present and pronounced not only in TMDCs but also in other materials with the direct band gap at the Brillouin zone boundary, e.g., hexagonal boron nitride *et al.* [61]. Topological resonances can also be present in materials where the direct band gap is not at one of the \mathcal{T} -invariant points such as the Γ point or the M points. The presence of a band gap is essential because it causes a gradual accumulation of the non-Abelian Berry phase along the Bloch \mathbf{k} -space electron trajectory, which is necessary to compensate the gradually accumulating dynamic phase.

The predicted induction of the valley polarization promises a wide range of important valleytronics applications, in particular, to PHz-band information processing and storage. The predicted topological resonance is a concept which will stimulate developments in topological strong-field optics of solids. In particular, the chiral, nonuniform electron distributions in the reciprocal space will cause chiral currents in the real space, which we will consider elsewhere.

Major funding was provided by Grant No. DE-FG02-01ER15213 from the Chemical Sciences, Biosciences and Geosciences Division, Office of Basic Energy Sciences, Office of Science, US Department of Energy. Numerical simulations have been performed using support by Grant No. DE-FG02-11ER46789 from the Materials Sciences and Engineering Division of the Office of the Basic Energy Sciences, Office of Science, US Department of Energy. The work of V.A. was supported by Grant No. ECCS-1308473 from US NSF. Support for S.A.O.M. came from a MURI Grant No. FA9550-15-1-0037 from the US Air Force Office of Scientific Research, and for J.-S.W. from a NSF EFRI NewLAW Grant No. EFMA-17 41691.

- [1] H. Fattahi, H. G. Barros, M. Gorjan, T. Nubbemeyer, B. Alsaif, C. Y. Teisset, M. Schultze, S. Prinz, M. Haefner, M. Ueffing, A. Alismail, L. Vamos, A. Schwarz, O. Pronin, J. Brons, X. T. Geng, G. Arisholm, M. Ciappina, V. S. Yakovlev, D.-E. Kim *et al.*, Third-generation femtosecond technology, *Optica* **1**, 45 (2014).
- [2] A. Schiffrin, T. Paasch-Colberg, N. Karpowicz, V. Apalkov, D. Gerster, S. Muhlbrandt, M. Korbman, J. Reichert, M. Schultze, S. Holzner, J. V. Barth, R. Kienberger, R. Ernstorfer, V. S. Yakovlev, M. I. Stockman, and F. Krausz, Optical-field-induced current in dielectrics, *Nature (London)* **493**, 70 (2012).
- [3] M. Schultze, E. M. Bothschafter, A. Sommer, S. Holzner, W. Schweinberger, M. Fiess, M. Hofstetter, R. Kienberger, V. Apalkov, V. S. Yakovlev, M. I. Stockman, and F. Krausz, Controlling dielectrics with the electric field of light, *Nature (London)* **493**, 75 (2013).
- [4] A. V. Mitrofanov, A. J. Verhoef, E. E. Serebryannikov, J. Lumeau, L. Glebov, A. M. Zheltikov, and A. Baltuška, Optical Detection of Attosecond Ionization Induced by a Few-Cycle Laser Field in a Transparent Dielectric Material, *Phys. Rev. Lett.* **106**, 147401 (2011).
- [5] E. Goulielmakis, V. S. Yakovlev, A. L. Cavalieri, M. Uiberacker, V. Pervak, A. Apolonski, R. Kienberger, U. Kleineberg, and F. Krausz, Attosecond control and measurement: Lightwave electronics, *Science* **317**, 769 (2007).
- [6] T. Paasch-Colberg, S. Y. Kruchinin, O. Saglam, S. Kapser, S. Cabrini, S. Muehlbrandt, J. Reichert, J. V. Barth, R. Ernstorfer, R. Kienberger, V. S. Yakovlev, N. Karpowicz, and A. Schiffrin, Sub-cycle optical control of current in a semiconductor: from the multiphoton to the tunneling regime, *Optica* **3**, 1358 (2016).
- [7] Q. H. Wang, K. Kalantar-Zadeh, A. Kis, J. N. Coleman, and M. S. Strano, Electronics and optoelectronics of two-dimensional transition metal dichalcogenides, *Nat. Nanotechnol.* **7**, 699 (2012).
- [8] L. Britnell, R. M. Ribeiro, A. Eckmann, R. Jalil, B. D. Belle, A. Mishchenko, Y. J. Kim, R. V. Gorbachev, T. Georgiou, S. V. Morozov, A. N. Grigorenko, A. K. Geim, C. Casiraghi, A. H. C. Neto, and K. S. Novoselov, Strong light-matter interactions in heterostructures of atomically thin films, *Science* **340**, 1311 (2013).
- [9] F. Withers, O. Del Pozo-Zamudio, A. Mishchenko, A. P. Rooney, A. Gholinia, K. Watanabe, T. Taniguchi, S. J. Haigh, A. K. Geim, A. I. Tartakovskii, and K. S. Novoselov, Light-emitting diodes by band-structure engineering in van der Waals heterostructures, *Nat. Mater.* **14**, 301 (2015).
- [10] G. B. Liu, D. Xiao, Y. G. Yao, X. D. Xu, and W. Yao, Electronic structures and theoretical modelling of two-dimensional group-VIB transition metal dichalcogenides, *Chem. Soc. Rev.* **44**, 2643 (2015).
- [11] K. S. Novoselov, A. Mishchenko, A. Carvalho, and A. H. C. Neto, 2D materials and van der Waals heterostructures, *Science* **353**, aac9439 (2016).
- [12] Y. Ye, J. Xiao, H. L. Wang, Z. L. Ye, H. Y. Zhu, M. Zhao, Y. Wang, J. H. Zhao, X. B. Yin, and X. Zhang, Electrical generation and control of the valley carriers in a monolayer transition metal dichalcogenide, *Nat. Nanotechnol.* **11**, 598 (2016).
- [13] H. Z. Liu, Y. L. Li, Y. S. You, S. Ghimire, T. F. Heinz, and D. A. Reis, High-harmonic generation from an atomically thin semiconductor, *Nat. Phys.* **13**, 262 (2017).
- [14] M. Ashton, J. Paul, S. B. Sinnott, and R. G. Hennig, Topology-Scaling Identification of Layered Solids and Stable Exfoliated 2D Materials, *Phys. Rev. Lett.* **118**, 106101 (2017).
- [15] M. C. Lemme, L.-J. Li, T. Palacios, and F. Schwierz, Two-dimensional materials for electronic applications, *MRS Bull.* **39**, 711 (2014).
- [16] K. S. Novoselov, V. I. Falko, L. Colombo, P. R. Gellert, M. G. Schwab, and K. Kim, A roadmap for graphene, *Nature (London)* **490**, 192 (2012).
- [17] D. Jariwala, V. K. Sangwan, L. J. Lauhon, T. J. Marks, and M. C. Hersam, Emerging device applications for semiconducting two-dimensional transition metal dichalcogenides, *ACS Nano* **8**, 1102 (2014).
- [18] A. K. Geim and K. S. Novoselov, The rise of graphene, *Nat. Mater.* **6**, 183 (2007).
- [19] F. Schwierz, Graphene transistors, *Nat. Nanotechnol.* **5**, 487 (2010).
- [20] G. B. Liu, W. Y. Shan, Y. G. Yao, W. Yao, and D. Xiao, Three-band tight-binding model for monolayers of group-VIB transition metal dichalcogenides, *Phys. Rev. B* **88**, 085433 (2013).
- [21] D. Xiao, G.-B. Liu, W. X. Feng, X. D. Xu, and W. Yao, Coupled Spin and Valley Physics in Monolayers of MoS₂ and Other Group-VI Dichalcogenides, *Phys. Rev. Lett.* **108**, 196802 (2012).
- [22] J. W. Jiang, Graphene versus MoS₂: A short review, *Front. Phys.* **10**, 287 (2015).
- [23] E. J. Sie, J. McIver, Y. H. Lee, L. Fu, J. Kong, and N. Gedik, Valley-selective optical stark effect in monolayer WS₂, *Nat. Mater.* **14**, 290 (2015).
- [24] H. L. Zeng, J. F. Dai, W. Yao, D. Xiao, and X. D. Cui, Valley polarization in MoS₂ monolayers by optical pumping, *Nat. Nanotechnol.* **7**, 490 (2012).
- [25] K. F. Mak, K. L. He, J. Shan, and T. F. Heinz, Control of valley polarization in monolayer MoS₂ by optical helicity, *Nat. Nanotechnol.* **7**, 494 (2012).
- [26] T. Cao, G. Wang, W. P. Han, H. Q. Ye, C. R. Zhu, J. R. Shi, Q. Niu, P. H. Tan, E. Wang, B. L. Liu, and J. Feng, Valley-selective circular dichroism of monolayer molybdenum disulphide, *Nat. Commun.* **3**, 887 (2012).
- [27] A. M. Jones, H. Y. Yu, N. J. Ghimire, S. F. Wu, G. Aivazian, J. S. Ross, B. Zhao, J. Q. Yan, D. G. Mandrus, D. Xiao, W. Yao, and X. D. Xu, Optical generation of excitonic valley coherence in monolayer WSe₂, *Nat. Nanotechnol.* **8**, 634 (2013).
- [28] M. Eginligil, B. C. Cao, Z. L. Wang, X. N. Shen, C. X. Cong, J. Z. Shang, C. Soci, and T. Yu, Dichroic spin-valley photocurrent in monolayer molybdenum disulphide, *Nat. Commun.* **6**, 7636 (2015).
- [29] See Supplemental Material at <http://link.aps.org/supplemental/10.1103/PhysRevB.98.081406> for detailed information about H^{TNN} , band structures of monolayers MoS₂ and WS₂ for spins up and down, the results for MoS₂ in the presence of two cycles of applied pulse, and the calculated valley and spin polarization as a function of field amplitude.
- [30] M. Garg, M. Zhan, T. T. Luu, H. Lakhotia, T. Klostermann, A. Guggenmos, and E. Goulielmakis, Multi-petahertz electronic metrology, *Nature (London)* **538**, 359 (2016).
- [31] P. Kroger, H. Suchowski, H. Liang, N. Flemens, K.-H. Hong, F. X. Kaertner, and J. Moses, Generation and multi-octave shaping

- of mid-infrared intense single-cycle pulses, *Nat. Photonics* **11**, 222 (2017).
- [32] H. Liang, P. Krogen, Z. Wang, H. Park, T. Kroh, K. Zawilski, P. Schunemann, J. Moses, L. F. DiMauro, F. X. Kaertner, and K.-H. Hong, High-energy mid-infrared sub-cycle pulse synthesis from a parametric amplifier, *Nat. Commun.* **8**, 141 (2017).
- [33] U. Elu, M. Baudisch, H. Pires, F. Tani, M. H. Frosz, F. Koettig, A. Ermolov, P. St.J. Russell, and J. Biegert, High average power and single-cycle pulses from a mid-ir optical parametric chirped pulse amplifier, *Optica* **4**, 1024 (2017).
- [34] C. Vicario, M. Shalaby, and C. P. Hauri, Subcycle Extreme Nonlinearities in Gap Induced by an Ultrastrong Terahertz Field, *Phys. Rev. Lett.* **118**, 083901 (2017).
- [35] S. S. Dhillon, M. S. Vitiello, E. H. Linfield, A. G. Davies, M. C. Hoffmann, J. Booske, C. Paoloni, M. Gensch, P. Weightman, G. P. Williams, E. Castro-Camus, D. R. S. Cumming, F. Simoens, I. Escorcia-Carranza *et al.*, The 2017 terahertz science and technology roadmap, *J. Phys. D: Appl. Phys.* **50**, 043001 (2017).
- [36] F. Langer, M. Hohenleutner, U. Huttner, S. W. Koch, M. Kira, and R. Huber, Symmetry-controlled temporal structure of high-harmonic carrier fields from a bulk crystal, *Nat. Photonics* **11**, 227 (2017).
- [37] J. Li, X. Ren, Y. Yin, Y. Cheng, E. Cunningham, Y. Wu, and Z. Chang, Polarization gating of high harmonic generation in the water window, *Appl. Phys. Lett.* **108**, 231102 (2016).
- [38] S. Sim, J. Park, J.-G. Song, C. In, Y.-S. Lee, H. Kim, and H. Choi, Exciton dynamics in atomically thin MoS₂: Interexcitonic interaction and broadening kinetics, *Phys. Rev. B* **88**, 075434 (2013).
- [39] G. Moody, J. Schaibley, and X. D. Xu, Exciton dynamics in monolayer transition metal dichalcogenides, *J. Opt. Soc. Am. B* **33**, C39 (2016).
- [40] Z. G. Nie, R. Long, L. F. Sun, C. C. Huang, J. Zhang, Q. H. Xiong, D. W. Hewak, Z. X. Shen, O. V. Prezhdo, and Z. H. Loh, Ultrafast carrier thermalization and cooling dynamics in few-layer MoS₂, *ACS Nano* **8**, 10931 (2014).
- [41] Y.-T. Wang, C.-W. Luo, A. Yabushita, K.-H. Wu, T. Kobayashi, C.-H. Chen, and L.-J. Li, Ultrafast multi-level logic gates with spin-valley coupled polarization anisotropy in monolayer MoS₂, *Sci. Rep.* **5**, 8289 (2015).
- [42] V. Apalkov and M. I. Stockman, Theory of dielectric nanofilms in strong ultrafast optical fields, *Phys. Rev. B* **86**, 165118 (2012).
- [43] V. Apalkov and M. I. Stockman, Metal nanofilm in strong ultrafast optical fields, *Phys. Rev. B* **88**, 245438 (2013).
- [44] T. Higuchi, M. I. Stockman, and P. Hommelhoff, Strong-Field Perspective on High-Harmonic Radiation from Bulk Solids, *Phys. Rev. Lett.* **113**, 213901 (2014).
- [45] H. K. Keldar, V. Apalkov, and M. I. Stockman, Wannier-Stark states of graphene in strong electric field, *Phys. Rev. B* **90**, 085313 (2014).
- [46] H. K. Keldar, V. Apalkov, and M. I. Stockman, Graphene in ultrafast and superstrong laser fields, *Phys. Rev. B* **91**, 045439 (2015).
- [47] H. K. Keldar, V. Apalkov, and M. I. Stockman, Ultrafast field control of symmetry, reciprocity, and reversibility in buckled graphene-like materials, *Phys. Rev. B* **92**, 045413 (2015).
- [48] H. K. Keldar, V. Apalkov, and M. I. Stockman, Attosecond strong-field interferometry in graphene: Chirality, singularity, and Berry phase, *Phys. Rev. B* **93**, 155434 (2016).
- [49] M. S. Wismer, S. Y. Kruchinin, M. Ciappina, M. I. Stockman, and V. S. Yakovlev, Strong-Field Resonant Dynamics in Semiconductors, *Phys. Rev. Lett.* **116**, 197401 (2016).
- [50] S. A. Oliaei Motlagh, V. Apalkov, and M. I. Stockman, Interaction of crystalline topological insulator with an ultrashort laser pulse, *Phys. Rev. B* **95**, 085438 (2017).
- [51] O. Kwon, T. Paasch-Colberg, V. Apalkov, B.-K. Kim, J.-J. Kim, M. I. Stockman, and D. E. Kim, Semimetallization of dielectrics in strong optical fields, *Sci. Rep.* **6**, 21272 (2016).
- [52] T. Higuchi, C. Heide, K. Ullmann, H. B. Weber, and P. Hommelhoff, Light-field-driven currents in graphene, *Nature (London)* **550**, 224 (2017).
- [53] F. Bloch, Über die Quantenmechanik der Elektronen in Kristallgittern, *Z. Phys. A* **52**, 555 (1929).
- [54] W. V. Houston, Acceleration of electrons in a crystal lattice, *Phys. Rev.* **57**, 184 (1940).
- [55] F. Wilczek and A. Zee, Appearance of Gauge Structure in Simple Dynamical Systems, *Phys. Rev. Lett.* **52**, 2111 (1984).
- [56] D. Xiao, M.-C. Chang, and Q. Niu, Berry phase effects on electronic properties, *Rev. Mod. Phys.* **82**, 1959 (2010).
- [57] F. Yang and R. B. Liu, Nonlinear optical response induced by non-Abelian Berry curvature in time-reversal-invariant insulators, *Phys. Rev. B* **90**, 245205 (2014).
- [58] A. A. Abrikosov, L. P. Gorkov, and I. E. Dzyaloshinski, *Methods of Quantum Field Theory in Statistical Physics* (Dover, New York, 1975).
- [59] W. Yao, D. Xiao, and Q. Niu, Valley-dependent optoelectronics from inversion symmetry breaking, *Phys. Rev. B* **77**, 235406 (2008).
- [60] Y. Liu, G. Bian, T. Miller, and T. C. Chiang, Visualizing Electronic Chirality and Berry Phases in Graphene Systems using Photoemission with Circularly Polarized Light, *Phys. Rev. Lett.* **107**, 166803 (2011).
- [61] M. S. Xu, T. Liang, M. M. Shi, and H. Z. Chen, Graphene-like two-dimensional materials, *Chem. Rev.* **113**, 3766 (2013).